Peptide-based microcapsules obtained by self-assembly and microfluidics as controlled environments for cell culture

Ferreira, DS; Reis, RL; Azevedo, HS

RSCPublishing **Soft Matter**

Peptide-based microcapsules obtained by self-assembly and microfluidics as controlled environments for cell culture

SCHOLARONE™
Manuscripts

Self-assembled peptide capsules allow co-culture of cells and control of cell-matrix interactions.
159x79mm (96 x 96 DPI)

Peptide-based microcapsules obtained by self-assembly and microfluidics as controlled environments for cell culture

Daniela S. Ferreira[1,2], Rui L. Reis[1,2], Helena S. Azevedo[1,2*]

[1] *3B's Research Group - Biomaterials, Biodegradables and Biomimetics, University of Minho, Headquarters of the European Institute of Excellence on Tissue Engineering and Regenerative Medicine, AvePark, 4806-909 Taipas, Guimarães, Portugal*

[2] *ICVS/3B's - PT Government Associate Laboratory, Braga/Guimarães, Portugal*

*corresponding author: hazevedo@dep.uminho.pt

Tel:+351 253 510 907, Fax: +351 253 510 909

Abstract

Peptides are excellent building blocks to form precise nanostructures by self-assembly. They can self-assemble into fibril nanostructures, thus recreating some of the architectural features of the natural extracellular matrix. Here, we used a microfluidic approach to drive the self-assembly of peptides of opposite charge into capsular structures for cell encapsulation. The obtained capsules presented a core shell structure made of a network of nanofibers and their properties can be tuned by varying the concentration of each peptide. Capsules were found to be stable in aqueous solutions and their permeability dependent on the capsule composition. Human dermal fibroblasts were encapsulated and remained viable within the capsules and their morphology was shown to be influenced by the matrix density. Additionally, these capsules also supported the co-culture of fibroblasts and keratinocytes. We expect that the developed peptide-based microcapsules can serve as miniaturized environments for cell culture and as biomimetic platforms for in vitro drug screening.

1. **Introduction**

Molecular self-assembly, the spontaneous organization of molecules into ordered aggregates by noncovalent interactions, is becoming increasingly important in the development of new biomaterials because it offers a great platform for constructing materials with high level of precision and complexity.[1, 2] Although bulk self-assembly of small molecules frequently yields structures that exhibit a high degree of order on the nanometer scale, they exhibit more disordered morphologies at the micrometer scale. However, recent research has demonstrated the feasibility of using electrostatic interactions between small molecules and high molecular weight polymers to drive their assembly into larger assemblies that can extend over multiple length scales.[3] On the other hand, directed self-assembly (DSA) has emerged as strategy to control order in materials across scales by tuning the directionally of self-assembly interactions at the nanoscale.[4] In DSA the positions of self-assembling building blocks are guided by an external input to introduce hierarchical organization in supramolecular materials. Examples of external inputs include mechanical forces, such as shear effects[5], magnetic[6] and electric[7] fields, thermal gradients[8] and chemically[9] or topographically[10] patterned substrates. Although the concept of DSA still remains ambiguous, templated self-assembly (TSA) can be considered as a kind of DSA, in which a prefabricated ''template'' orients and directs the assembling components.[11] Another approach towards DSA is the use of geometric confinement to orient bulk structures or to induce the formation of novel morphologies not found in bulk systems. For example, microfluidics has been used to guide the self-assembly of block copolymers,[12] and in the synthesis of liposomes[13] and microcapsules,[14] thus providing additional control over the size and shape of self-assembled structures.

It is widely understood that in order to encapsulate living cells within an artificial matrix, the encapsulating conditions must not damage the cells and the matrix material must be biocompatible and at the same time provide a natural microenvironment for the cells to sustain their viability, function and growth. The mechanical strength of the encapsulating matrix is also critical for maintaining the matrix integrity and to withstand manipulations associated with *in vitro* culture. Moreover, it is essential that the matrix should have suitable diffusion properties to ensure sufficient access of nutrients, for encapsulated cells to remain viable and functional, and the removal of secreted metabolic waste products. Thus, there is a need for relatively mild cell encapsulation methods, which offers control over properties of the encapsulating matrix. An exciting approach for cell encapsulation is the use of materials that can undergo gelation in cell-compatible conditions. Hydrogels are appealing for cell encapsulation because they are highly hydrated three-dimensional networks that provide an environment for cells to adhere, proliferate, and differentiate and they can often be processed under relatively mild conditions. Gelation can occur through a change in temperature, or via chemical crosslinking, ionic crosslinking, or formation of an insoluble complex.[15]

Self-assembling materials, not depending on covalent chemistry, enable the direct cell encapsulation under mild conditions. Within self-assembled nanomaterials, peptide nanostructures can present varied geometries (e.g. micelles, nanofibers, vesicles)[16, 17] and chemical diversity for biological recognition. Peptides are, therefore, excellent structural units to form complex nanostructures that can recreate some of the architectural features and functionalities of the natural extracellular matrix (ECM).

Previous work from the Stupp lab demonstrated the self-assembly of peptide-amphiphile (PA) molecules of opposite charges into nanofibers by electrostatic attraction at neutral pH.[18] Mixing solutions of oppositely charged PAs resulted in nanofiber formation and at certain concentration transformed into a 3D gel. Ionic interactions between positively charged and negatively charged moieties within the peptides has been explored as a self-assembly mode.[19-21]

Cell microencapsulation is a technology with enormous clinical potential for the production of biologically important therapeutics and the treatment of a wide range of diseases.[22] The encapsulation of cells in microscopic gel capsules can also be used for exploratory purposes in biology, to study the role of specific microenvironments on cell fate, create cell arrays for single-cell bioassays and for drug screening.[23] To optimize the performance of microgel capsules, it is crucial to control size, shape and the content of encapsulated additives. The use of emulsion droplet as templates for microgel synthesis has been widely explored.[23-25] The principle of this technique is to use micrometer-scale channels to carry a solution of a microgel precursor. The stream of the precursor solution can be broken up by flow focusing with continuous phase of an immiscible fluid, normally an oil phase. When these two fluids meet, droplets are formed, drop-by-drop, due to the interfacial tension and the shear of the continuous phase. By varying the microchannel geometry, the flow rates and viscosities of the fluids, monodisperse droplets with controlled size can be generated. The subsequent droplet gelation allows retaining their morphology. Thus, the main goal of the present study was to produce soft peptide microgel capsules with controlled properties for cell encapsulation and culture. Towards this goal, we used droplet-based microfluidics to guide the electrostatic self-assembly of peptides of opposite charge and generate

capsules with controlled spherical shape and monodisperse size. The structure and properties of the obtained peptide capsules are described, as well as their application as 3D matrix for conducting different cell culture studies (e.g. cell-matrix interactions, co-culture).

2. Materials and methods

Peptide synthesis and purification

Two peptide amphiphiles (PAs) with opposite charge were synthesized in this work, consisting of a peptide segment covalently linked to a 16-carbon alkyl chain: C_{16}-$V_3A_3K_3$ (K_3-PA) and C_{16}-$V_3A_3E_3$ (E_3-PA) (Fig. 1). The peptides were synthesized on a CS Bio 136XT automated peptide synthesizer (CS Bio, USA) using standard 9-fluorenylmethoxycarbonyl (Fmoc) based solid phase chemistry. K_3-PA was synthesized on a 4-methylbenzhydrylamine (MBHA) rink amide resin (Novabiochem, Germany) and E_3-PA on a 4-benzyloxybenzylamine Wang resin pre-loaded with the first glutamic acid (Fmoc-Glu(OtBu)-Wang resin). Amino acid couplings were performed using 4 equivalents (4 mmol) of Fmoc protected amino acids (Novabiochem, Germany), 4 equivalents of O-(Benzotriazol-1-yl)-N,N,N',N'-tetramethyluronium hexafluorophosphate (HBTU, Novabiochem®) and 6 equivalents of N,N-diisopropylethylamine (DIEA, Sigma, USA). Fmoc deprotections were performed with 20% piperidine (Sigma, USA) in dimethylformamide. A palmitic acid ($C_{16}H_{32}O_2$, Calbiochem, Germany) tail was manually coupled under the same conditions as the Fmoc-amino acids. Peptide cleavage from the resin and removal of the protecting groups was carried out on a mixture of trifluoroacetic acid (TFA, Sigma, USA)/triisopropylsilane (TIS, Alfa Aesar)/water (95/2.5/2.5)) for 3 h at room temperature. The peptide mixture was collected and excess of TFA was removed by rotary evaporation. The resulting viscous peptide solution was triturated with cold diethyl ether and the white precipitate was collected by filtration, washed with cold ether, and allowed to dry under vacuum overnight. The peptide mass was confirmed by matrix assisted laser desorption/ionization mass spectrometry (MALDI-MS, 4800

MALDI-TOF/TOF, AbSciex). Peptides were then purified on a Waters 2545 Binary Gradient high-performance liquid chromatography (HPLC) system using preparative reverse-phase C_{18} columns. K_3-PA was purified on an Atlantis Prep OBD T3 column (Waters) with a water/acetonitrile (0.1% TFA) gradient and E_3-PA on a Xbridge column (Waters) with a water/acetonitrile (0.1% NH_4) gradient. For K_3-PA, TFA counter-ions were exchanged by sublimation from 0.01 M hydrochloric acid. Finally, the peptides were dialyzed against ultrapure water using 500 MWCO dialysis tubing (Spectrum labs, The Netherlands), lyophilized and stored at -20 ºC until further use. Confirmation of mass and purity was done by MALDI-MS and HPLC (Supplementary Information, Fig. S1-S2). Peptide solutions used in cell culture studies were sterilized by UV exposure for 15 minutes.

Preparation of peptide-based capsules

Capsules were generated using a microfluidic device developed in our lab that allows the production of stable and size-controlled spherical capsules.[26] This system can be conveniently cleaned and sterilized allowing cell encapsulation in a sterile environment, reducing contamination risks during the procedure. A solution of E_3-PA (1 wt%) in 0.15 M NaCl was first and injected into one of the microchannels of the microfluidics device using a syringe pump (Alladdin WPI, England). Simultaneously, mineral oil was provided to the oil microchannel from a reservoir using a low speed peristaltic pump (Ismatec, Switzerland). The operation rates of the peristaltic and syringe pumps were set at 50 μL/min and 20 μL/min, respectively. The peptide microdroplets were generated inside the microfluidics device by shear stress when the E_3-PA solution in the horizontal microchannel entered into the stream of mineral oil in

the larger vertical microchannel (Fig. 1A). The formed microdroplets were collected

from the outlet tubing in a separate vessel containing 1 mL of K_3-PA solution (0.1, 0.2

and 0.5 wt%) in 0.1 M $CaCl_2$. 10 μL of Tween-80 was added as a surface-active agent to

prevent aggregation of the capsules. Capsules were incubated in the K_3-$CaCl_2$ solution

for 15 minutes and washed three times with 0.15 M NaCl.

Capsule characterization

Phase contrast microscopy

Microscopic observations of the capsules were carried out to examine their size and

shape. Phase contrast micrographs of the capsules were acquired in an inverted

microscope (Axio Observer, Zeiss, Germany). The size of the capsules was then

estimated by measuring the diameter of individual capsules (n=30).

Scanning electron microscopy (SEM)

The microstructure of the capsules was analyzed by SEM. Samples were fixed in a 2%

glutaraldehyde/3% sucrose in PBS for 1 h at 4 ºC followed by sequential dehydration in

graded ethanol concentrations (from 20 to 100%). To remove ethanol, samples were

dried in a Tousimis Autosandri®-815 (series A) critical point dryer. To expose the

internal surface of the capsules, they were cut into half with a sharp blade. Prior

observation, the samples were coated with a gold/palladium layer and imaged using

an ultra-high resolution field emission gun scanning electron microscope (Nova™

NanoSEM 200) from FEI (Eindhoven, The Netherlands).

Swelling

The stability of the capsules in aqueous environment was studied by incubating them in water and PBS. Capsules (n=10/well, in triplicate) prepared with 0.1, 0.2 and 0.5% K_3-PA were distributed in a 24 well plate and 1 mL of ultrapure water or PBS was added to each well. Samples were incubated at 37 ºC and at predetermined time points (1, 2, 3 and 7 days) capsules were observed in an inverted microscope (Axio Observer, Zeiss, Germany) and their size was measured using ZEN software (Zeiss, Germany) .

Mechanical stability

To study the mechanical stability of the different capsules, 10 capsules (in triplicate) were placed in 12 well plates containing 2 mL of PBS and 10 glass beads (3 mm diameter, VWR) . The plate was placed in a flat rotator (DSR-2800 V, Digisystem Laboratory Instruments Inc., Taiwan) shaking at about 200 rpm. At predetermined time points (2, 4 6 and 24 h), the number of intact capsules was counted by observation in an inverted microscope (Axio Observer, Zeiss, Germany). The percentage of intact capsules as a function of time was determined by calculating the ratio between the number of intact capsules at each time point and the initial number.

Permeability

The capsule permeability was investigated by using dextran standards of different molecular weights (20, 40 and 155 kDa). For that, FITC- and TRITC-labeled dextrans (Sigma, USA) were encapsulated within the capsules and their release followed along the time. Three different solutions were prepared; each solution was a mixture of 0.5 mg/mL of dextran (20, 40 and 155 kDa) with 1 wt% E_3-PA. The mixture was injected into the microfluidic device and capsules were generated as described before. The

capsules were then placed in PBS (pH 7.4) at 37 ºC in a water bath with agitation. At specific time intervals, the release medium was completely collected for further analysis and replaced with the same amount of fresh PBS solution. The fluorescence was measured at 485/528 nm (FITC-labeled) and 530/590 nm (TRITC-labeled) on a microplate reader (BIO-TEK, Synergie HT, USA). The concentration of released dextran was measured using a calibration curve using known concentrations of dextran solutions.

Cell culture and encapsulation

Isolation and culture of human dermal fibroblasts and epidermal keratinocytes

Human dermal fibroblasts (hDFb) and epidermal keratinocytes (hKc) were isolated from skin samples discarded from abdominoplasty surgeries of consenting patients at Hospital da Prelada (Porto, Portugal). Briefly, the skin tissue was cut in pieces of 0.5 by 0.5 cm and digested in a dispase solution (2.4 U/mL in PBS) at 4 ºC, overnight. After dissociation of the epidermis from the dermis, keratinocytes were isolated by a 5 minute digestion of the epidermis in 0.25% trypsin/EDTA (Invitrogen, UK) at 37 ºC to release the cells. Trypsin was inactivated by the addition of the same volume of fetal bovine serum (FBS, Gibco, UK), the digestion products were poured through a 100 µm cell strainer and centrifuged at 200 g for 5 minutes. Cell pellet was washed with phosphate buffered saline (PBS, Gibco, UK)) and centrifuged at 200 g for 5 minutes. The pellet was resuspended and the cells were subsequently cultured in Keratinocyte Serum Free Medium (KSFM, Gibco, UK) with L-glutamine and keratinocyte-SFM supplement (Gibco, UK), in a 37 ºC humidified atmosphere with 5% CO_2. Fibroblasts were isolated from the dermis by overnight digestion of the dermal pieces in a

collagenase IA solution (125 U/mL in PBS) at 4 ºC. Digestion products were poured through a 100 μm cell strainer and centrifuged at 200 g for 5 minutes. The pellet was resuspended and the cells were subsequently cultured in Dulbecco's Modified Eagle Medium (DMEM) (Sigma, Germany) supplemented with 10% FBS (Gibco, UK) and 1% (v/v) antibiotic/antimycotic solution (A/B) (Gibco, UK) containing 100 units/mL penicillin and 100 mg/mL streptomycin, in a 37 ºC humidified atmosphere with 5% CO_2. Cells used in this study were between passage 2 and 4 (hDFb) and passage 1 and 2 (hKc).

Encapsulation and culture of hDFb within capsules

Confluent hDFb were harvested from monolayer cultures using trypsin-EDTA (Invitrogen, USA). Cells were washed in PBS and centrifuged at 200 g for 10 minutes to remove calcium residues from the medium. Cell pellet was then resuspended at a density of 1.0 x 10^6 cells/mL in 1 wt% E_3-PA solution. Capsules were generated as described before, using a 0.1 wt% K_3-PA solution supplemented with 0.1 M $CaCl_2$. Capsules were transferred to 24-well plates and cultured up to 14 days in DMEM without phenol red (Sigma) supplemented with 10% FBS (Gibco, UK) and 1% (v/v) A/B (Gibco, UK), in a 37 ºC humidified atmosphere with 5% CO_2. Fibroblast morphology and interaction with the artificial matrix were also investigated as a function of matrix composition by varying E_3-PA concentration. Cell pellet was resuspended at a density of 1.0x10^6 cells/mL in E_3-PA solutions (0.5, 1 and 2 wt%) in NaCl. At predetermined time points, samples were collected to assess cell viability (live/dead assay), morphology and spreading (SEM, F-actin and collagen I staining).

Live/Dead staining

Cell viability was assessed through live/dead assay using calcein-AM (Sigma) and propidium iodide (PI, Molecular Probes, Invitrogen, USA) dyes. Calcein-AM is a membrane-permeant dye, which is hydrolyzed by endogenous esterase into the highly negatively charged green fluorescent cell marker calcein retained in the cytoplasm. Propidium iodide is a membrane impermeant, thus binding to DNA of dead cells. At each time point, medium was removed and 1 mL of PBS containing 2 μL of calcein-AM and 1 μL of PI was added to each well. Samples were incubated for 10 minutes at 37 ºC protected from light followed by three washes in PBS, and were immediately visualized in a fluorescence microscope (Axioimage RZ1M, Zeiss, Germany).

Staining and confocal microscopy

For examining the morphology of encapsulated hDFbs within the different capsules, staining for collagen I and e F-actin was carried out after fixing cells in 10% formalin solution (Sigma-Aldrich, Germany) for 30 minutes at 4 ºC. Cells were then washed once with 0.1 M Glycine in PBS and twice with PBS and permeabilized with 2% BSA/ 0.2% Triton X-100 solution for 1 h at RT. Samples were incubated with primary antibody anti-collagen I (ab292, 1:500, abcam, UK) for 1 h at RT and washed three times for 2 minutes with PBS. Samples were then incubated with the secondary antibody, anti-mouse Alexa 488 (1:200, Molecular Probes, Invitrogen, USA) for 1 h at RT. In some cases, samples were treated with TRITC-conjugated phalloidin (1 U/mL, Sigma-Aldrich, Germany) for 1 h at RT. Cell nuclei were counterstained with 1 mg/mL DAPI (1:1000, Sigma-Aldrich, Germany) for 1 min and washed with PBS. Visualization was performed by confocal laser scanning microscopy (CLSM,Olympus FluoView 1000, Olympus,

Japan). Background was subtracted and images were processed using FV10-ASW 3.1

software (Olympus, Japan).

Cell proliferation

Cell proliferation within the capsules was assessed at different culture times (1, 3, 7

and 14 days) by quantifying the amount of double-stranded DNA (dsDNA). Samples

were prepared as described elsewhere[27]. Briefly, capsules were lyophilized and

resuspended in phosphate-buffered EDTA (pH 6.5) supplemented with 0.01 M L-

cysteine (Sigma, USA) and 0.5% papain (Sigma, USA). Digestion was performed at 60 ºC

for 24 h. Following this, quantification was performed using the Quant-iT™ PicoGreen®

dsDNA Assay Kit (Invitrogen, Molecular Probes, Oregon, USA), according to the

instructions of the manufacturer. The fluorescent intensity of the dye was measured in

a microplate reader (Synergie HT, Bio-Tek, USA) with excitation at 485/20 nm and

emission at 528/20 nm. The DNA concentration for each sample was calculated using a

standard curve (DNA concentration ranging from 0 to 1.5 mg/mL) relating quantity of

DNA and fluorescence intensity. The fluorescence signals obtained from blank capsules

(i.e. without cells, cultured and processed similarly to those with cells) were used as

background values (blanks). Triplicates were made for each time point and for each

sample (n=10 capsules/sample).

Co-culture studies - seeding of keratinocytes on the surface of the capsules with encapsulated fibroblasts

To validate our peptide capsules for co-culture studies, hDFb and hKc were co-cultured

within and on the capsule surface, respectively. Encapsulation of hDFb capsules was

processed as described previously. Capsules were transferred to 6-well plates and cultured in DMEM without phenol red, supplemented with 10% FBS and 1% A/B. After 1 day, keratinocytes were seeded on the capsules (5×10^5 cells/well) and cultured on a 25:75 mixture (previously optimized in monoculture) of DMEM (containing 10% FBS, 1% A/B) and keratinocyte serum free medium with supplements in a 37 ºC humidified atmosphere with 5% CO_2. Cells were examined under SEM to analyze cell morphology and cell-matrix interactions. Samples were fixed, dehydrated and prepared as described for SEM analysis. Co-cultured cells were also characterized using an immunocytochemistry assay with specific markers for each cell type. Samples were fixed and prepared as described previously. The primary antibodies and dilutions used in the assay were anti-fibroblast surface protein (F4771, 1:500, Sigma, USA) and anti-keratin 5 (PRB-160P, 1:500, Covance, Spain). The secondary antibodies and dilutions were anti-rabbit Alexa 488 (1:200) and anti-mouse Alexa 594 (1:500) (Molecular Probes, Invitrogen, USA). Samples were visualized by CLSM (Olympus FluoView 1000, Olympus, Japan). Background was subtracted and images were processed using FV10-ASW 3.1 software (Olympus, Japan).

Data analysis and statistics

All data values are presented as mean ± standard deviation (SD). Statistical analysis was performed using GraphPad Prism 5.00 software (San Diego, USA). Statistical differences were determined using one-way analysis of variance (ANOVA) with a Bonferroni's multiple comparisons post-hoc test (Permeability, DNA quantification). Differences between groups in the mechanical stability study were determined using a

two-way analysis of variance (ANOVA) with a Bonferroni's multiple comparisons post-hoc test. ($*$ $p < 0.05$, $**$ $p < 0.01$ and $***$ $p < 0.001$)

3. Results and discussion

Building blocks for electrostatic driven-self-assembly

The self-assembling peptides used in this study are amphiphilic molecules, composed of a hydrophobic segment coupled to a peptide sequence, that includes a β-sheet forming sequence (VVVAAA) and a domain with charged amino acids, either positive (KKK, K_3-PA, Fig. 1B) or negative (EEE, E_3-PA, Fig. 1A).[27]

The negatively charged peptide (E_3-PA) was chosen by its known ability to undergo self-assembly into nanofribrillar structures in the presence of divalent cations, such as Ca^{2+}, and form stable gels at certain concentrations.[8, 27, 28] It has been shown that self-assembling peptide gels present a nanofibrillar network that resemble de structural architecture of extracellular matrix, making them attractive for studying cell-matrix interactions on a 3D environment.[29-31] Electrostatic-driven self-assembly between PAs of opposite charge was demonstrated by the formation of nanofibers with subsequent formation of self-supporting gels.[18] Based on these findings, we hypothesized that microfluidic technology could be used to control the size and microscopic shape of nanostructures generated by electrostatic self-assembly. Peptide droplets generated in the microfluidic device would serve as templates to produce spherical capsular structures by self-assembly (Fig. 1). The core and shell of the proposed capsules can be further tailored by changing the peptide concentration and/or the conditions during the self-assembly process, for example the pH, as it is known that pH affects the charge of peptides. For example, Savin and Doyle[19] studied the effect of pH on the kinetics of self-assembly of a model peptide containing positively charged and

negatively charged residues. Using multiple particle tracking, they found that increasing the pH of the peptide solution from 3.5 to 4.0, the gelation time decreased by almost hundredfold. By incorporating bioactive moieties in the peptide sequences, these peptide capsules can offer a versatile artificial matrix to encapsulate cells and study their behavior under different physical and biochemical signals.

Capsule generation by directed self-assembly

In the present work, we have used a microfluidic method to generate spherical capsular structures by self-assembly between oppositely charged peptides for the encapsulation of human dermal fibroblasts.

The first step in capsule preparation requires the formation of microdroplets of an aqueous solution of a negatively charged peptide (E_3-PA, 1 wt%) in the microfluidic device through emulsification in the oil phase (Fig. 1A). The E_3-PA microdroplets were then directly extruded into a solution of a similar peptide with opposite charge (Fig. 1B). The peptide microdroplets formed in the oil phase served as templates for the formation of stable spherical capsules by electrostatic self-assembly between the E_3 and K_3 PAs. The microfluidics device was used to control/guide the interfacial self-assembly between the two peptides to obtain a final microstructure with a spherical shape, instead their "chaotic" self-assembly in solution. Here, the shape and size of the peptide droplet, formed in the microfluidic device, determines the final morphology of the assembly. At the droplet interface, self-assembly immediately occurs resulting on the formation of a capsular structure (a wall membrane made of K_3-E_3-PA nanofibers with a liquefied core containing free E_3-PA molecules – Fig. 1C). The oil phase separates from the K_3-PA solution and floats to the surface because of the difference in densities. This phase

separation allows the aqueous peptide droplets to be dispersed in the K_3-PA solution (below the oil phase). The mineral oil is removed from the collection vessel by pipetting out the upper layer. The K_3-PA solution was supplemented with 0.1 M $CaCl_2$ to induce the gelation of internal E_3-PA (Fig. 1D). To further control the microstructure and permeability of the capsule wall, the concentration of K_3-PA was varied (0.1, 0.2, 0.5 wt%).

The morphology and microstructure of the generated capsules were analyzed with phase contrast microscopy and SEM. Their stability, mechanical resistance, permeability and ability to support the encapsulation and survival of human dermal fibroblasts were also studied.

Capsule characterization

Size, morphology and microstructure

Images obtained by phase contrast microscopy showed spherical shaped capsules with uniform size and a diameter of around 1000 µm (Fig. 2A). Higher concentrations of K_3-PA (> 1 wt%) generated larger capsules with a dense shell that would difficult the diffusion of nutrients and cell metabolites, leading to the formation of necrotic centers and cell death. On the other hand, lower concentrations, ranging from 0.1 to 0.5 wt%, resulted in stable capsules. SEM micrographs of the capsules showed a shell with a nanofibrillar structure (Fig. 2B) as a result from the self-assembly between the peptides. The external surface of the capsules exhibit a network of nanofibers randomly distributed but the nanofiber density was higher for the capsules formed at higher concentration of K_3-PA. This observation showed that we were able to modulate capsule shell microstructure by varying K_3-PA concentration, which may have

implications on the capsule permeability. Furthermore, this external membrane enables the protection of encapsulated species from the external environment. The capsules can have either a liquid (Fig. 1C) or gel core after gelation with Ca^{2+} ions (Fig. 1D), allowing to create different cellular microenvironments, either for culturing cells in suspension or anchorage-dependent cells. Liquid core capsules were less stable and more susceptible to burst, whereas core gelation generates robust capsules using concentrations of E_3-PA from 0.5 to 2 wt%. To assess the internal surface, capsules were fractured before SEM imaging. SEM micrographs showed a dense core with a random fibrillar structure (Fig. 2C).

Swelling, mechanical stability and permeability

A general requirement for capsules as 3D environments for cell encapsulation and culture include their mechanical and chemical stability in aqueous media (e.g. buffer, cell culture medium). To investigate whether capsules were able to maintain their structural integrity when exposed to aqueous solutions, capsules were incubated in water or PBS and their size variation was followed for 7 days. Capsules were shown to be very stable in both solutions, without relevant size variation along time (Fig. 3A). Capsules with lower swelling rate are less prone to rupture and to induce an inflammatory response when implanted *in vivo*.[32] To evaluate capsules mechanical stability, an additional study was performed. Capsules were incubated in PBS with glass beads under agitation and their membrane integrity was followed for 24 h. As expected, capsules formed at higher concentration of K_3-PA (0.5 wt%), with a denser outer shell, showed to be less prone to damage (Fig. 3B), although the difference between conditions is more notorious only after 24 h.

Capsules permeability is crucial for cell encapsulation to allow the diffusion of oxygen, nutrients and cell metabolites. Additionally, when used for cell delivery therapies, they should also be able to avoid the influx of immune cells and antibodies. To assess the effect of K_3-PA concentration on the permeability of the capsules, dextran standards of different molecular weights (20, 40, 155 kDa) were encapsulated within the capsules and their release followed with time. The release profile of 20 kDa dextran was similar for all the conditions and faster than the dextran with higher MW, as expected, and after 24 h about 60% of the encapsulated dextran was released from the capsules (Fig. 3C). For the 40 kDa dextran, a similar behavior was observed for the capsules with 0.1 and 0.2 wt% K_3-PA. After 24 h, about 50% of the encapsulated dextran was released. The percentage of dextran released from the capsules formed with 0.5 wt% K_3-PA was lower (40%) as expected (Fig. 3C). The diffusion of the higher MW dextran (155 kDa) was slower. After 24 h, only 20-25% of the encapsulated dextran was released in all the conditions (Fig. 3C). These results indicate that capsules formed in higher peptide concentration exhibit a controlled diffusion of high molecular weight molecules.

This difference in the capsule permeability may be related to their microstructure observed by SEM (Fig. 3C, Fig. S3). Capsules formed with higher concentration of K_3-PA showed a shell structure with a much denser nanofibrillar organization which may hamper the diffusion of larger molecules. Estimation of the porosity of the capsule external surface also confirmed higher porosity for the capsules prepared with lower peptide concentrations (Supplementary Information, Fig. S4). By varying the concentration of one of the components (K_3-PA) we were able to modulate the capsule wall porosity and permeability.

Encapsulation and culture of hDFb within capsules

Most of cell-matrix interactions *in vivo* occur in 3D environments, with the cells normally embedded within an ECM that is constantly undergoing remodelling by the cells themselves. The potential of the developed capsules as 3D scaffolds for anchorage-dependent cells was investigated by the encapsulation of human dermal fibroblasts.

Cell viability and proliferation

A fluorescence live/dead assay was performed to assess the viability of encapsulated cells. Living (green) cells with well-defined round contours were visualized and no dead cells (shown as red nuclei) were detected within the capsules. Furthermore, cells remained viable and well distributed within the capsules throughout the 14 days of culture (Fig. 4B).

The quantification of DNA (Fig. 4A) revealed a gradual increase in DNA as a result of fibroblast proliferation over time. These results demonstrate that the capsule composition and the method to obtain them did not affect cell viability.

Expression of collagen I

Fibroblasts have the natural ability to remodel their extracellular microenvironment by either expressing proteolytic enzymes or synthesizing ECM proteins, such as collagen I.[33] The ability of fibroblasts to synthesize collagen I was assessed by immunofluorescence, as an indirect way to evaluate encapsulated fibroblasts functionality. Confocal microscopy images showed that cells maintained the ability to produce collagen I during the culture time (Fig. 4C2,C3).

Cell morphology

The morphology of fibroblasts within the capsules was assessed by SEM. Micrographs showed round-shaped cells in the capsules inside cavities, that reflect the living spaces preserved by the cells (Fig. 4D). In the SEM images, cell size can be estimated to be around 10 µm. A thin fiber-like matrix secreted by the cells was visible shortly after one day. The presence of these protrusions was more evident after 14 days of culture, showing the interaction of the fibroblasts with the nanofibrillar structure of the gelled E_3-PA. Although fibroblasts were still interacting with the fibrillar matrix of the self-assembled peptide, cells still remained round after 14 days of culture. Based on this observation, and previous findings on the effect of matrix properties on fibroblast proliferation in 3D gels,[34] which showed that at higher stiffness the matrix acts as physical barrier for cells in 3D, impeding their proliferation and migration, we have further investigated the influence of peptide concentration inside the capsules on the morphology of encapsulated fibroblasts.

Influence of matrix composition on fibroblast morphology

Fibroblast morphology and cell-matrix interactions were investigated by varying the percentage of E_3-PA (0.5, 1 and 2 wt%) inside the capsule. Previous studies using collagen matrices prepared under diverse conditions showed that matrix stiffness increases with matrix density.[35] Here, we intended to modulate the matrix density in the capsules core by varying peptide concentration. SEM micrographs of the capsules interior confirmed our hypothesis revealing a higher density of fibrillar nanostructures with increasing concentration of E_3-PA (Fig. 5A). SEM micrographs of encapsulated

fibroblasts within 1 and 2 wt% E_3-PA showed round shaped cells interacting with the nanofibrillar structure of the gelled peptide, similar to what we have observed before (Fig. 5B). In contrast, within 0.5 wt% E_3-PA capsules, cells remained round after 1 day, but after 7 days, fibroblasts had spread out exhibiting extended protrusions interacting with fibrillar structure of E_3-PA. When cultured in 0.5 wt% E_3-PA, cells adopted a spindle shape with fine filopodia. After 14 days, the spread cells formed a 3D-network and phalloidin-stained F-actin showed highly elongated cells with clearly-defined stress fibers (Fig. 5C). In contrast, cells cultured in 1 and 2 wt% E_3-PA capsules maintained a spherical shape, and phalloidin staining showed peripheral deposition or poorly organized F-actin that followed the cell contours. As previously observed, fibroblasts maintained their ability to synthesize collagen I. Within 0.5 wt% E3-PA capsules, collagen I has a strong signal and was well distributed in the cytosol, whereas in 1 and 2 wt% E_3-PA the signal was weaker and collagen distribution was more peripheral. These results show a similar trend to what has been observed by Bott and co-authors,[34] when studying the effect of matrix stiffness on fibroblast proliferation in 3D gels. It has been shown that fibroblasts normally exhibit a flat morphology with dorsal-ventral polarity and extended protrusions when cultured in 2D[36, 37] because when they migrate and proliferate they do not experience major physical barriers.[38] However, when encapsulated in a 3D matrix, fibroblasts need to overcome barriers posed by the surrounding environment to proliferate and migrate, re-acquiring a natural spindle-shaped morphology.[36-38] These results highlight the role of the core matrix density/stiffness in controlling cell morphology and cell-matrix interaction.

Co-culture studies – culture of hKC over the surface of the peptide capsules encapsulating hDFb

In vitro co-culture systems, using relevant cell types, can serve as mimics of tissue niches found *in vivo* and be used as valuable tools for probing and manipulating cell-cell interactions. Since interactions between cells can occur through soluble factors via paracrine signaling, co-culture studies should be performed in interactive microenvironments to permit the exchange of soluble factors between neighboring cells, while maintaining the different cells physically separated. In addition, these microenvironments should recreate the composition and structure of native ECMs. By using gelled core peptide capsules with a fibrillar structure, we have demonstrated that hDFb could be encapsulated within the capsules and were able to survive for 14 days. To further demonstrate the ability of these capsular structures for conducting more complex cellular studies (e.g. co- culture) we investigated their ability to support the co-culture of hDFb and hKc, within and on the capsule surface, respectively (Fig. 6A). The hKc gradually adhered to the capsule surface and covered it after 24 h, resulting in hDFb-hKC co-cultured capsules, as seen in phase contrast microscopy images (Fig. 6B1). Confocal microscopy images of the capsules stained with antibodies specific for each cell type (Fig. 6B2-B4), showed that co-cultured capsules consisted of encapsulated fibroblasts within the E_3-PA fibrillar matrix (Fig. 6B3), confined by a layer of keratinocytes on the outer shell (Fig. 6B2). SEM micrographs showed that keratinocytes were fully adhered to the capsule shell, exhibiting extended filopodia and lamellipodia and interacting with the fibrillar surface of K_3-PA (Fig. 6C). Our results showed that these capsules represent a good model to resemble the three-dimensional architecture of *in vivo* tissues carrying different cell types. In addition,

these peptide-based capsules can be tailored in a highly controlled manner to mimic ECM properties and functions. For example, the peptides in the capsule outer shell and core can be customized for other cell types by incorporating specific peptide sequences and their composition can be tuned to obtain matrices with defined structure and stiffness for 3D cell culture.

4. Conclusions

Here we demonstrate the application of electrostatic self-assembly, between peptide amphiphiles, combined with microfluidics to guide the assembly into spherical capsules. These capsules present a core shell structure and their properties (nanofibrillar density, permeability, stiffness) can be tuned by varying the concentration of each peptide. By controlling the capsules properties, cell-matrix interactions can be studied in a 3D environment. Capsules composed of a simple negatively charged peptide, without any cell-adhesive sequence, were shown to support the survival of encapsulated human dermal fibroblasts. Another application of these capsules is demonstrated by co-culturing two cell types within and on their surface. The versatility of the selected building blocks to present bioactive ligands provides the opportunity to mimic other functionalities of the natural ECM, which can find numerous applications in cell biology and regenerative medicine.

5. References

1.   T. Aida, E. W. Meijer and S. I. Stupp, *Science*, 2012, **335**, 813-817.
2.   S. I. Stupp, *Nano Lett*, 2010, **10**, 4783-4786.
3.   R. M. Capito, H. S. Azevedo, Y. S. Velichko, A. Mata and S. I. Stupp, *Science*, 2008, **319**, 1812-1816.
4.   R. Haghgooie and P. S. Doyle, *Soft Matter*, 2009, **5**, 1192-1197.
5.   C. W. Wang, D. Sinton and M. G. Moffitt, *Acs Nano*, 2013, **7**, 1424-1436.
6.   D. W. P. M. Lowik, I. O. Shklyarevskiy, L. Ruizendaal, P. C. M. Christianen, J. C. Maan and J. C. M. van Hest, *Adv Mater*, 2007, **19**, 1191-+.
7.   Y. S. Velichko, J. R. Mantei, R. Bitton, D. Carvajal, K. R. Shull and S. I. Stupp, *Adv Funct Mater*, 2012, **22**, 369-377.
8.   S. M. Zhang, M. A. Greenfield, A. Mata, L. C. Palmer, R. Bitton, J. R. Mantei, C. Aparicio, M. O. de la Cruz and S. I. Stupp, *Nat Mater*, 2010, **9**, 594-601.
9.   K. Sugihara, M. Chami, I. Derenyi, J. Voros and T. Zambelli, *Acs Nano*, 2012, **6**, 6626-6632.
10.   A. C. Mendes, K. H. Smith, E. Tejeda-Montes, E. Engel, R. L. Reis, H. S. Azevedo and A. Mata, *Adv Funct Mater*, 2013, **23**, 430-438.
11.   B. A. Grzybowski, C. E. Wilmer, J. Kim, K. P. Browne and K. J. M. Bishop, *Soft Matter*, 2009, **5**, 1110-1128.
12.   R. Karnik, F. Gu, P. Basto, C. Cannizzaro, L. Dean, W. Kyei-Manu, R. Langer and O. C. Farokhzad, *Nano Lett*, 2008, **8**, 2906-2912.
13.   A. Jahn, S. M. Stavis, J. S. Hong, W. N. Vreeland, D. L. DeVoe and M. Gaitan, *Acs Nano*, 2010, **4**, 2077-2087.
14.   A. C. Mendes, E. T. Baran, P. Lisboa, R. L. Reis and H. S. Azevedo, *Biomacromolecules*, 2012, **13**, 4039-4048.
15.   D. Seliktar, *Science*, 2012, **336**, 1124-1128.
16.   E. Gazit, *Nat Chem*, 2010, **2**, 1010-1011.
17.   E. Gazit, *Chem Soc Rev*, 2007, **36**, 1263-1269.
18.   K. L. Niece, J. D. Hartgerink, J. J. J. M. Donners and S. I. Stupp, *J. Am. Chem. Soc.*, 2003, **125**, 7146-7147.
19.   T. Savin and P. S. Doyle, *Soft Matter*, 2007, **3**, 1194-1202.
20.   M. R. Caplan, P. N. Moore, S. G. Zhang, R. D. Kamm and D. A. Lauffenburger, *Biomacromolecules*, 2000, **1**, 627-631.
21.   S. G. Zhang, T. Holmes, C. Lockshin and A. Rich, *Proc. Natl. Acad. Sci. U. S. A.*, 1993, **90**, 3334-3338.
22.   T. M. S. Chang, *Nat Rev Drug Discov*, 2005, **4**, 221-235.
23.   D. Velasco, E. Tumarkin and E. Kumacheva, *Small*, 2012, **8**, 1633-1642.
24.   S. Allazetta, T. C. Hausherr and M. P. Lutolf, *Biomacromolecules*, 2013.
25.   S. Seiffert, *Chemphyschem*, 2013, **14**, 295-304.
26.   A. C. Mendes, E. T. Baran, R. L. Reis and H. S. Azevedo, *Acta Biomater.*, 2013, **9**, 6675-6685.
27.   M. J. Webber, J. Tongers, M.-A. Renault, J. G. Roncalli, D. W. Losordo and S. I. Stupp, *Acta Biomater.*, 2010, **6**, 3-11.
28.   E. T. Pashuck, H. G. Cui and S. I. Stupp, *J. Am. Chem. Soc.*, 2010, **132**, 6041-6046.
29.   E. Beniash, J. D. Hartgerink, H. Storrie, J. C. Stendahl and S. I. Stupp, *Acta Biomater.*, 2005, **1**, 387-397.
30.   S. G. Zhang, *Nat. Biotechnol.*, 2003, **21**, 1171-1178.
31.   M. Zhou, A. M. Smith, A. K. Das, N. W. Hodson, R. F. Collins, R. V. Ulijn and J. E. Gough, *Biomaterials*, 2009, **30**, 2523-2530.
32.   M. D. Darrabie, W. F. Kendall Jr and E. C. Opara, *Biomaterials*, 2005, **26**, 6846-6852.

33.   A. D. Metcalfe and M. W. Ferguson, *J R Soc Interface*, 2007, **4**, 413-437.
34.   K. Bott, Z. Upton, K. Schrobback, M. Ehrbar, J. A. Hubbell, M. P. Lutolf and S. C. Rizzi, *Biomaterials*, 2010, **31**, 8454-8464.
35.   B. A. Roeder, K. Kokini, J. E. Sturgis, J. P. Robinson and S. L. Voytik-Harbin, *J Biomech Eng*, 2002, **124**, 214-222.
36.   K. M. Yamada and E. Cukierman, *Cell*, 2007, **130**, 601-610.
37.   E. Cukierman, R. Pankov, D. R. Stevens and K. M. Yamada, *Science*, 2001, **294**, 1708-1712.
38.   P. Friedl and E. B. Bröcker, *CMLS, Cell. Mol. Life Sci.*, 2000, **57**, 41-64.

Figure 1. Capsule generation by directed self-assembly. Schematic representation of the set-up for capsule generation and cell encapsulation. The E_3-PA microdroplets generated at the T-junction of the microfluidic system (A) were directly extruded into a solution of K_3-PA for electrostatic self-assembly (B). At the droplets interface, self-assembly immediately occurs resulting on the formation of a capsular structure (a wall membrane made of K_3-E_3-PA nanofibers with a liquefied core containing free E_3-PA molecules (C). The K_3-PA solution was supplemented with 0.1 M $CaCl_2$ to induce the gelation of internal E_3-PA (D).

Figure 2. Capsules morphology and microstructure. Phase contrast microscopy images (A) and SEM micrographs (B) showing the size and overall structure of peptide-based capsules. SEM micrographs of capsule shell at higher magnification show a network of nanofibers randomly distributed with higher density for the capsules with higher concentration of K_3-PA. SEM micrographs of capsule interior show a dense core with a random fibrillar structure (C).

Figure 3. Capsules stability and permeability. Capsules stability in aqueous solutions (A) and mechanical resistance (B) as a function of K_3-PA concentration. Capsule permeability assessed by the release of encapsulated dextran (fluorescently labeled) with different molecular weights (20, 40 and 155 kDa) (C). Scanning electron micrographs shows differences in network morphology and fiber density that depend on K3-PA concentration. (**) $p < 0.01$, (*) $p < 0.05$, error bars represent standard deviation

Figure 4. *In* vitro viability and proliferation of hDFb encapsulated within peptide-based capsules. Cell proliferation assessed by dsDNA quantification (A) ((***) $p< 0.001$, (*) $p< 0.05$, error bars represent standard deviation (n=3)) and fluorescence microscopy images of live/dead assay on encapsulated fibroblasts (B). Living cells were stained by calcein (green) and dead cells by propidium iodide (red). Scale bar represents 200 μm. Phase contrast microscopy of encapsulated fibroblasts in the capsules (C1) and confocal microscopy images of stained collagen I produced by hDFb during culture time (C2, C3). SEM micrographs of encapsulated cells show round-shaped cells inside cavities (D).

Figure 5. Influence of matrix composition on fibroblast morphology. SEM micrographs of the capsules interior revealed a higher density of fibrillar nanostructures with increasing concentration of E_3-PA (A). Morphology of hDFb cultured within the peptide capsules revealed by SEM at day 14 (inset image shows the morphology of the cells at day 1) (B). Confocal microscopy images of stained collagen I (green) and f-actin (red) after 14 days, showed spread cells that formed a 3D-network with highly elongated cells in 0.5% E3-PA capsules (C). Cells cultured in 1 and 2 wt% E_3-PA capsules maintained a spherical shape, with peripheral deposition or poorly organized F-actin that followed the cell contours.
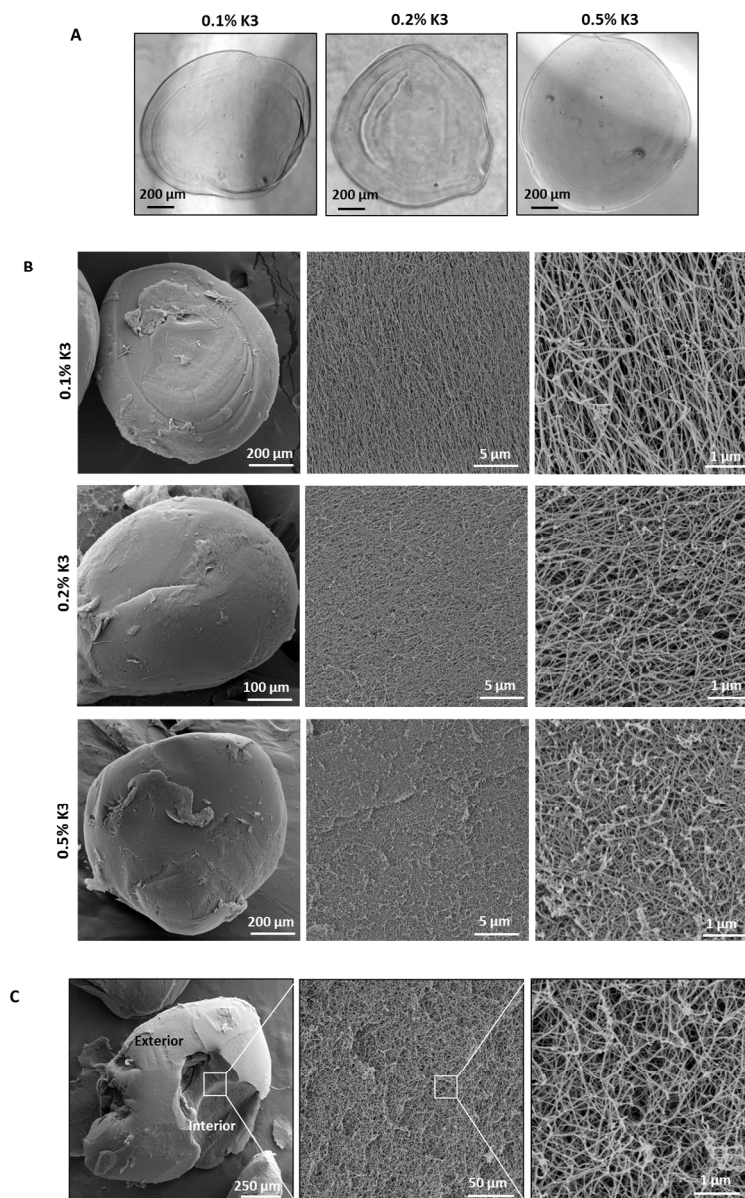
Figure 6. Co-culture studies. Concept of co-culturing skin cells within and on the peptide-based capsules (A). Phase contrast image showing keratinocytes on the capsule surface (B1). Immunostaining of specific markers for each cell type confirmed the localization of the fibroblasts in the capsule interior (B3) and keratinocytes on the

surface (B2). SEM micrographs show keratinocytes fully adhered to the capsule shell, exhibiting extended filopodia and lamellipodia and interacting with the fibrillar surface (C).
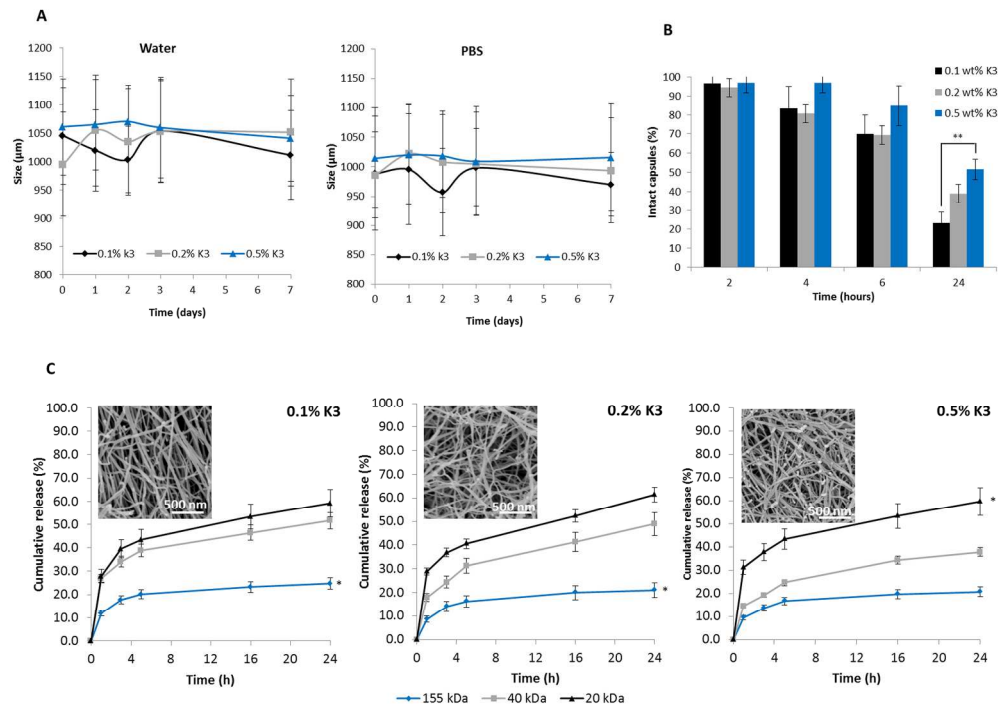
Capsule generation by directed self-assembly. Schematic representation of the set-up for capsule generation and cell encapsulation. The E3-PA microdroplets generated at the T-junction of the microfluidic system (A) were directly extruded into a solution of K3-PA for electrostatic self-assembly (B). At the droplets interface, self-assembly immediately occurs resulting on the formation of a capsular structure (a wall membrane made of K3-E3-PA nanofibers with a liquefied core containing free E3-PA molecules (C). The K3-PA solution was supplemented with 0.1 M CaCl2 to induce the gelation of internal E3-PA (D).

148x82mm (300 x 300 DPI)

Capsules morphology and microstructure. Phase contrast microscopy images (A) and SEM micrographs (B) showing the size and overall structure of peptide-based capsules. SEM micrographs of capsule shell at higher magnification show a network of nanofibers randomly distributed with higher density for the capsules with higher concentration of K3-PA. SEM micrographs of capsule interior show a dense core with a random fibrillar structure(C).
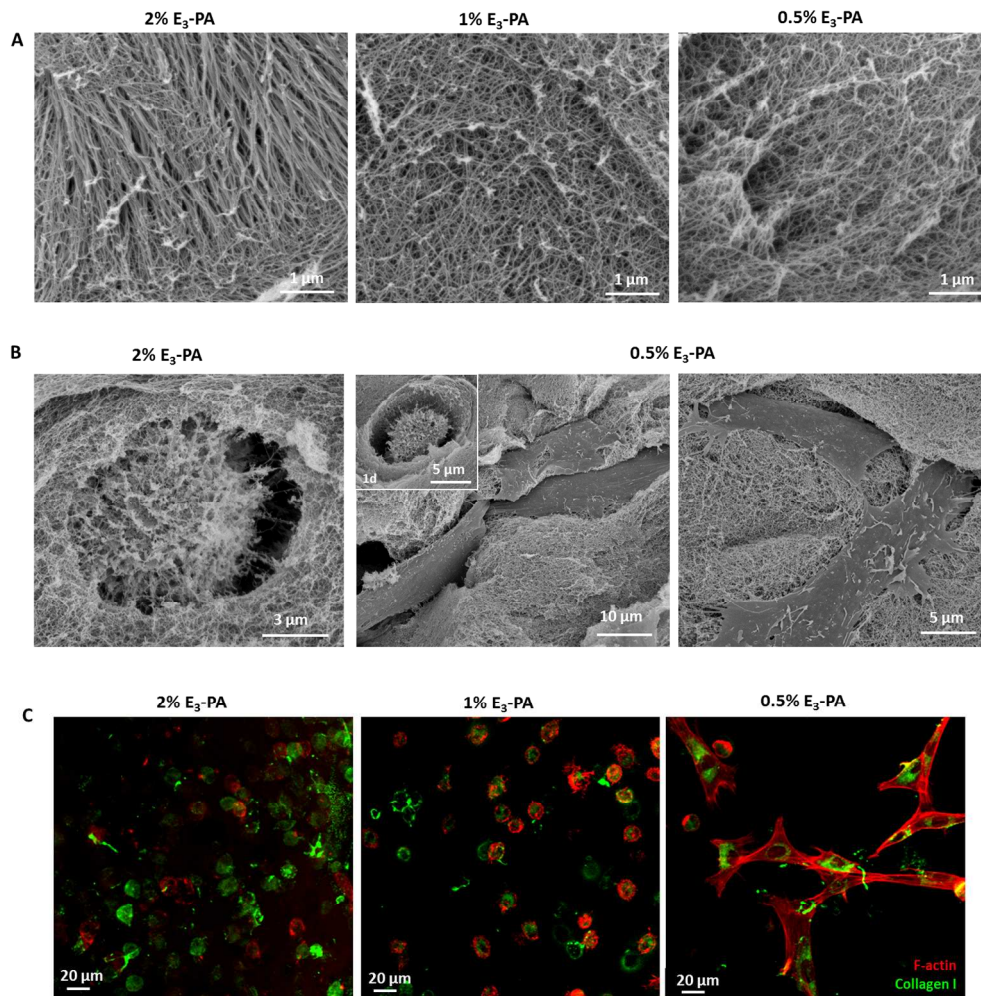
217x340mm (300 x 300 DPI)

Capsules stability and permeability. Capsules stability in aqueous solutions (A) and mechanical resistance (B) as a function of K3-PA concentration. Capsule permeability assessed by the release of encapsulated dextran (fluorescently labeled) with different molecular weights (20, 40 and 155 kDa) (C). Scanning electron micrographs shows differences in network morphology and fiber density that depend on K3-PA concentration. (**) p< 0.01, (*) p< 0.05, error bars represent standard deviation
213x151mm (300 x 300 DPI)

In vitro viability and proliferation of hDFb encapsulated within peptide-based capsules. Cell proliferation assessed by dsDNA quantification (A) ((***) p< 0.001, (*) p< 0.05, error bars represent standard deviation (n=3)) and fluorescence microscopy images of live/dead assay on encapsulated fibroblasts (B). Living cells were stained by calcein (green) and dead cells by propidium iodide (red). Scale bar represents 200 μm. Phase contrast microscopy of encapsulated fibroblasts in the capsules (C1) and confocal microscopy images of stained collagen I produced by hDFb during culture time (C2, C3). SEM micrographs of encapsulated cells show round-shaped cells inside cavities (D).
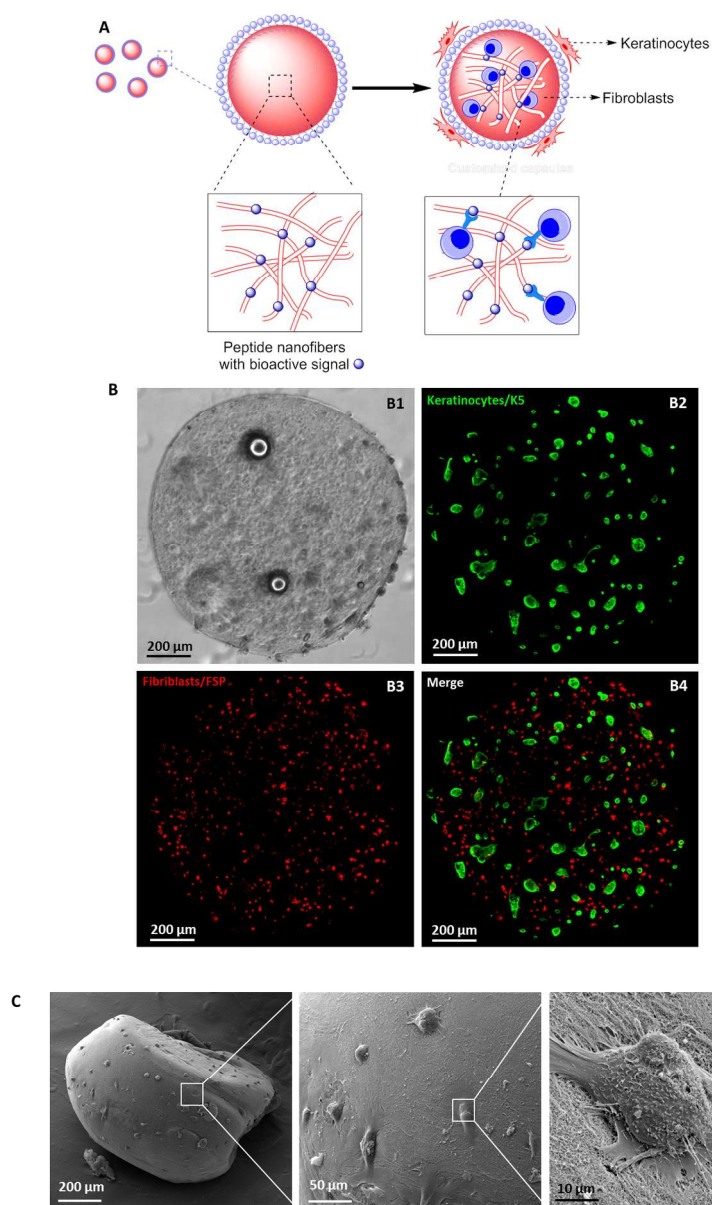
249x346mm (300 x 300 DPI)

Influence of matrix composition on fibroblast morphology. SEM micrographs of the capsules interior revealed a higher density of fibrillar nanostructures with increasing concentration of E3-PA (A). Morphology of hDFb cultured within the peptide capsules revealed by SEM at day 14 (inset image shows the morphology of the cells at day 1) (B). Confocal microscopy images of stained collagen I (green) and f-actin (red) after 14 days, showed spread cells that formed a 3D-network with highly elongated cells in 0.5% E3-PA (C). Cells cultured in 1 and 2 wt% E3-PA capsules maintained a spherical shape, with peripheral deposition or poorly organized F-actin that followed the cell contours.

256x256mm (300 x 300 DPI)

Co-culture studies. Concept of co-culturing skin cells within and on the peptide-based capsules (A) Phase contrast image showing keratinocytes on the capsule surface (B1). Immunostaining of specific markers for each cell type confirmed the localization of the fibroblasts in the capsule interior (B3) and keratinocytes on the surface (B2). SEM micrographs show keratinocytes fully adhered to the capsule shell, exhibiting extended filopodia and lamellipodia and interacting with the fibrillar surface (C).
228x346mm (300 x 300 DPI)

Supplementary Information

Peptide-based microcapsules obtained by self-assembly and microfluidics as

controlled environments for cell culture

Daniela S. Ferreira[1,2], Rui L. Reis[1,2], Helena S. Azevedo[1,2]

[1] *3B's Research Group - Biomaterials, Biodegradables and Biomimetics, University of Minho, Headquarters of the European Institute of Excellence on Tissue Engineering and Regenerative Medicine, AvePark, 4806-909 Taipas, Guimarães, Portugal*
[2] *ICVS/3B's - PT Government Associate Laboratory, Braga/Guimarães, Portugal*

All peptides were synthesized, characterized and purified successfully. MALDI-MS was used to characterize the mass of the synthesized peptides (Fig. S1-S2, A).

The expected mass for $C_{16}V_3A_3K_3$ ($C_{58}H_{111}N_{13}O_{10}$) was 1150.58, two main peaks were found by MALDI-MS, corresponding to [M] m/z = 1150.84, and $[M+Na]^+$ m/z= 1172.83 (Fig. S1A).
The expected mass for $C_{16}V_3A_3E_3$ ($C_{55}H_{95}N_9O_{17}$) was 1152.68, one main peak was found by MALDI-MS, m/z = 1152.80(Fig. S2A).

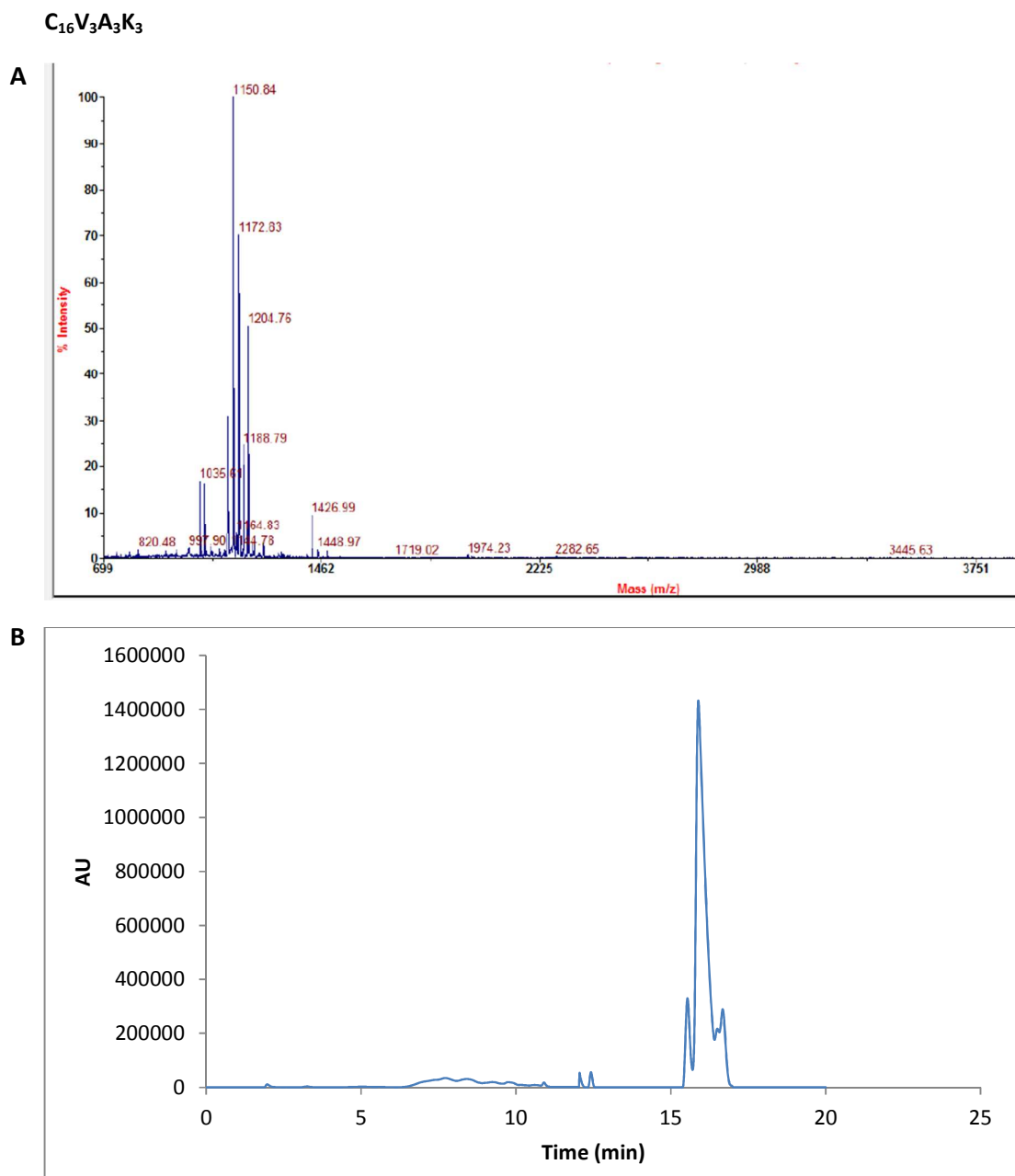Analytical HPLC of the collected fractions showed a single peak after purification for all the PAs (Fig. S1-S2, B)

$C_{16}V_3A_3K_3$

Figure S1. Representative MALDI-MS data (A) and analytical HPLC trace, detected at 220 nm (B) of $C_{16}V_3A_3K_3$.

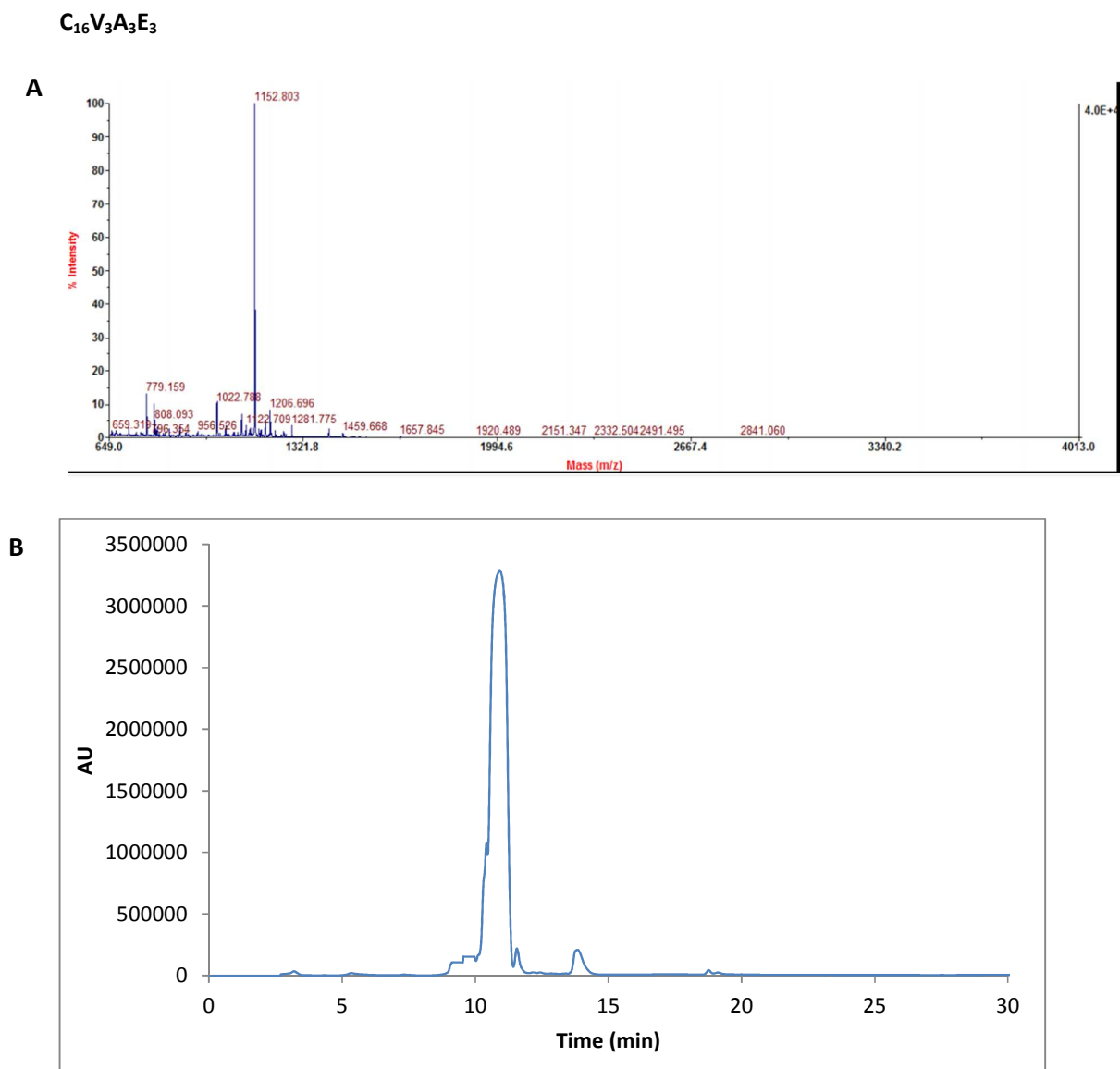$C_{16}V_3A_3E_3$

A

B

Figure S2. Representative MALDI-MS data (A) and analytical HPLC trace, detected at 220 nm (B) of $C_{16}V_3A_3E_3$.
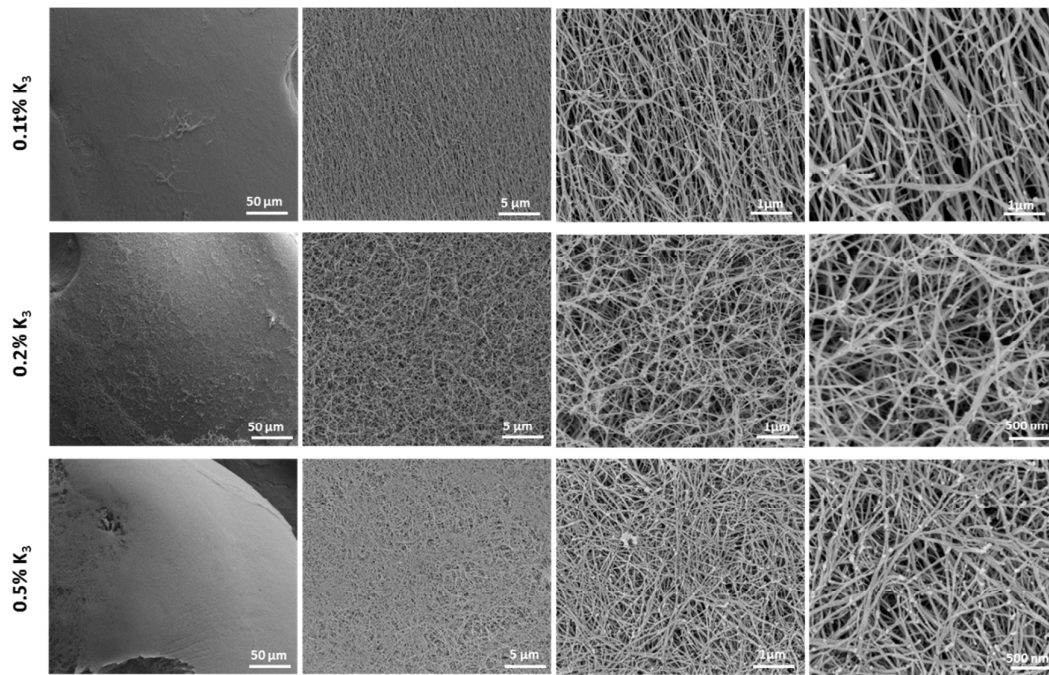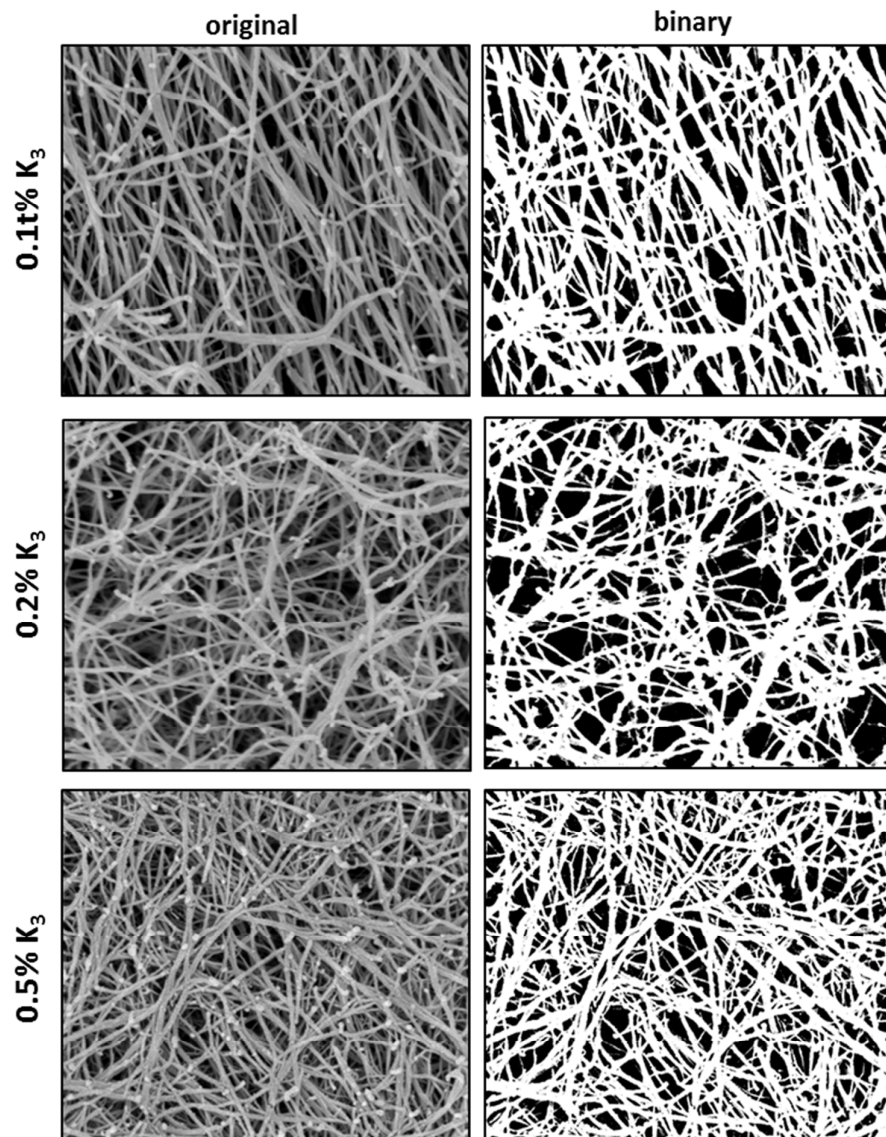
Figure S3. SEM micrographs of capsule external surface at different magnifications and as function of K3-PA concentration.

Capsule shell porosity was estimated using SEM micrographsa nd ImageJ sotware (NIH, USA) for image analysis and processing.[S1] To separate the nanofibers from the background, a threshold was set to the image by assigning the pixels in the image as either completely white or black. Once the range was selected a binary image was created (Fig. S4) by the software in which objects (nanofibers) are white and background is black. The measurement tool was then used to quantify the area covered by the pores or by the nanofibers. Since the image area was known, the area fraction filled by the pores was calculated giving an estimated value of porosity.

%K3	Estimated Porosity (%)
0.1	64.4
0.2	41.6
0.5	23.1

Figure S4. SEM micrographs of external surface of capsules prepared at different K_3-PA concentrations and thresholded images processed with ImageJ software (A). Estimated porosity of capsule shell as function of K_3-PA concentrations.

References

S1. J. Farmer, B. Duong, S. Seraphin, S. Shimpalee, M. J. Martinez-Rodriguez, J. W. Van Zee, *J. Power Sources*, 2012, **197**,1-11.